Boost of cosmetic active ingredient penetration triggered and controlled by the delivery of kHz plasma jet on human skin explants

Vinodini Vijayarangan, Sébastien Dozias, Catherine Heusèle, Olivier Jeanneton, Carine Nizard, Chantal Pichon, Jean Michel Pouvesle, Augusto Stancampiano, Eric Robert

frontiers | Frontiers in Physics

TYPE Original Research
PUBLISHED 11 April 2023
DOI 10.3389/fphy.2023.1173349

OPEN ACCESS

EDITED BY
XinPei Lu,
Huazhong University of Science and Technology, China

REVIEWED BY
Lanlan Nie,
Huazhong University of Science and Technology, China
Zhitong Chen,
Shenzhen Institute of Advanced Technology (CAS), China

*CORRESPONDENCE
Eric Robert,
eric.robert@univ-orleans.fr

SPECIALTY SECTION
This article was submitted to Low-Temperature Plasma Physics, a section of the journal Frontiers in Physics

RECEIVED 24 February 2023
ACCEPTED 27 March 2023
PUBLISHED 11 April 2023

CITATION
Vijayarangan V, Dozias S, Heusèle C, Jeanneton O, Nizard C, Pichon C, Pouvesle JM, Stancampiano A and Robert E (2023), Boost of cosmetic active ingredient penetration triggered and controlled by the delivery of kHz plasma jet on human skin explants.
Front. Phys. 11:1173349.
doi: 10.3389/fphy.2023.1173349

Boost of cosmetic active ingredient penetration triggered and controlled by the delivery of kHz plasma jet on human skin explants

Vinodini Vijayarangan[1,2,3], Sébastien Dozias[2], Catherine Heusèle[3], Olivier Jeanneton[3], Carine Nizard[3], Chantal Pichon[2,4], Jean Michel Pouvesle[1], Augusto Stancampiano[1] and Eric Robert[1]*

[1]GREMI UMR7344, CNRS/Université d'Orléans, Orléans, France, [2]Centre de Biophysique Moléculaire (CBM), CNRS UPR, Orléans, France, [3]LVMH Recherche, Saint Jean de Braye, France, [4]Institut Universitaire de France, Paris, France

This work reports on the demonstration of the penetration of cosmetic active ingredients (caffeine and hyaluronic acid) in human skin explants following safe and controlled plasma jet exposure. First, temperature increase and immunohistochemistry in the *stratum corneum* and epidermis were characterized to check the safe delivery of plasma jets and to select two operation regimes at 1 and 20 kHz. Plasma exposure for tens of seconds is shown to induce transient modulations of skin pH, transepidermal water loss, and skin wettability, revealing a reversible skin barrier function modulation. Then, it is demonstrated that plasma exposure significantly accelerates the penetration of active ingredients. The tuning of the plasma jet pulse repetition rate allows controlling the penetration kinetics. Such *ex vivo* results agree with previous *in vitro* experiments also exhibiting a transient permeabilization time window. A preliminary demonstration of human skin wettability modulation with a low-power, user-friendly dielectric barrier discharge setup is documented, opening perspectives for plasma-based home cosmetic care device development. To the best of our knowledge, this work is one of the first demonstrations of safe and controlled plasma-assisted active ingredients' skin penetration in the context of cosmetic applications.

KEYWORDS

non-thermal plasma, cosmetics, skin barrier, skin penetration and permeability, skin penetration kinetics, hyaluronic acid, caffeine, plasma jet

1 Introduction

The cosmetics industry is a key technological sector and a huge and fast-growing business market [1] with constant innovation, new consumers, and recent trends to promote, among others, natural ingredients, personalized cosmetics, safety, cosmetic active-ingredient efficiency, and new vectorization alternatives of cosmetic ingredients. Such new vectorization may rely on the new formulations and/or their coupling with new physical devices likely to promote their efficient, controlled, and safe usage. Physical vectorization for cosmetics or drugs has been considered with transdermal patches [2], microneedles [3–5], ultrasound applicators [6–8],

iontophoresis [9], electroporation [10], magnetophoresis [11], and skin treatment with lasers [12]. Even more recently, non-thermal physical plasma technology, which already showed interesting results in dermatology, is currently being studied for its potential in skin treatment and care. Non-thermal plasmas produced by gas discharge excitation and delivered in ambient air generate various biologically active species [13–15] together with charged species, ultraviolet light, a modest thermal load, and transient electric fields [16–18]. In the perspective of skin therapies, such plasmas have already demonstrated potent action in the acceleration of wound healing or skin disease treatments, e.g., for psoriatic or vitiligous lesions [19–25]. Skin cell stimulation with action on motility and proliferation was also reported [25, 26]. Non-thermal plasmas can also modify the pH of skin or any other target, and this effect was documented during clinical trials on intact human skin [27, 28]. They also have potent disinfecting action that is likely to have a positive role in the treatment of some skin diseases [29–32]. Plasmas have been demonstrated to destabilize the skin barrier, leading to water loss [33] or, conversely, trigger a strong increase in the *stratum corneum* wettability [34]. A recent review on the very first demonstration, perspectives, and challenges on the use of cold atmospheric pressure plasma for drug delivery for therapeutic clinical applications beyond the dermatological area was reported in Refs. [35, 36]. A comprehensive review of the potentialities of non-thermal plasmas for various skin treatments has also been recently published [37].

Nevertheless, there are very few reports on the development of non-thermal plasma for cosmetic application, including safety and biologically assessed and controlled actions on skin tissues except some perspective papers [38, 39]. The challenges are numerous, with the mandatory need to develop a safe plasma delivery protocol to control the reactive species generation by putting plasma in contact with different skin types in various environments. If cosmetic ingredient uptake enhancement is the objective, the control of the penetration depth and kinetics following plasma application should also be studied and controlled.

In this work, the development of a helium plasma jet to promote the penetration of relevant molecules for cosmetics is studied. All the results are obtained and analyzed from *ex vivo* human skin treatments, and both the safety and performance of plasma delivery are assessed. In Section 2, materials (plasma set up, skin samples, and cosmetic ingredients) and methods, including physicochemical skin surface characterization and biological skin tissue analysis, are described. Section 3 presents the results for successively skin temperature, transepidermal water loss, skin pH, and wettability modulation following plasma treatment and the potentialities for cosmetic ingredient uptake enhancement. The very preliminary and prospective development of a low-power dielectric barrier discharge (DBD) applicator and its interaction with human skin is finally introduced. The last section (Section 4) addresses the main conclusions and briefly introduces the bridges with an iontophoresis approach.

2 Materials and methods

2.1 Plasma setups and treatment conditions

Figure 1 illustrates the plasma device, the skin samples, and the plasma–skin sample exposure setup. In this work, the non-thermal plasma device used for skin explant exposure is the so-called "plasma gun", developed at GREMI for years for biomedical applications [40]. A borosilicate capillary with 4/6 mm for inner/outer diameters, respectively, flushed with 0.5 slm of helium (Alphagaz 1 Air Liquide, France), is equipped with an inner hollow powered electrode and an outer ring grounded electrode. The power supply generates a voltage pulse of 2 µs full width at half maximum with a Gaussian shape and a peak amplitude of either 10 or 14 kV delivered at a 1 or 20 kHz repetition frequency. Typical delivered powers measured when a plasma jet impinges on an agarose gel sample mimicking a human skin target with the Lissajous plot method are 0.045 and 0.9 W for 1 and 20 kHz, respectively [41]. The tip of the capillary is tapered with an inner diameter at the outlet of 1.4 mm so that the helium gas flow velocity is enhanced with the benefit of the cooling of the target.

Temperature measurements are performed with a 200-µm diameter fiber optics-based Optocon® device having an accuracy of 0.2°C. The tip of the probe fiber was exposed to the plasma jet at various distances from the capillary nozzle and for various pulse repetition rates. The probe was located near the plasma jet exposure area on the skin surface. While intrusively exposed, the dielectric nature and the small diameter of the probe were important features to achieve a representative and reliable temperature measurement.

Two protocols for plasma exposure of the skin samples have been selected from the initial studies documented in Section 3.1. They will be mentioned as 1k100s and 20k50s in the following and, respectively, correspond to a 1 kHz repetition rate for 100 s treatment with a distance of 1 cm from the sample to the capillary outlet and 20 kHz, 50 s, 1.5 cm setting.

As documented in Section 3.4, preliminary and prospective validations that results obtained with the plasma jet could be translated with the use of an air dielectric barrier discharge have been performed. The plasma ball model SP001 (Buki store, France) was used. The outer glass bulb was removed with the objective of using the inner part of the device. This inner part is basically the assembly of a high-frequency antenna covered with a spherical glass envelope. When approaching the glass envelope a few mm from the hand or knee of the operator, a very faint DBD discharge is ignited in the air gap. No fine control of the operation of the DBD device was desired, the main goal being to use a cheap, very low power, and user-friendly system likely to help design a prototype for future cosmetic home care applications. Only the author's hands and knee short-time exposures were performed. This work definitively does not claim to be a clinical demonstration, the latter requiring a mandatory volunteer recruitment protocol and a detailed risk assessment analysis for the plasma delivery, which are far beyond the scope of this preliminary study.

2.2 Skin sample conditioning and preparation for analysis

A first set of explants were issued from plasties, residues from esthetic abdominal surgery (Proviskin, Besançon, France). Plasties from patients not older than 50 years, samples exhibiting no scars or stretch marks, and with phototype I or II have been used in this work. Skin samples were dermatomized to a thickness of 500 µm,

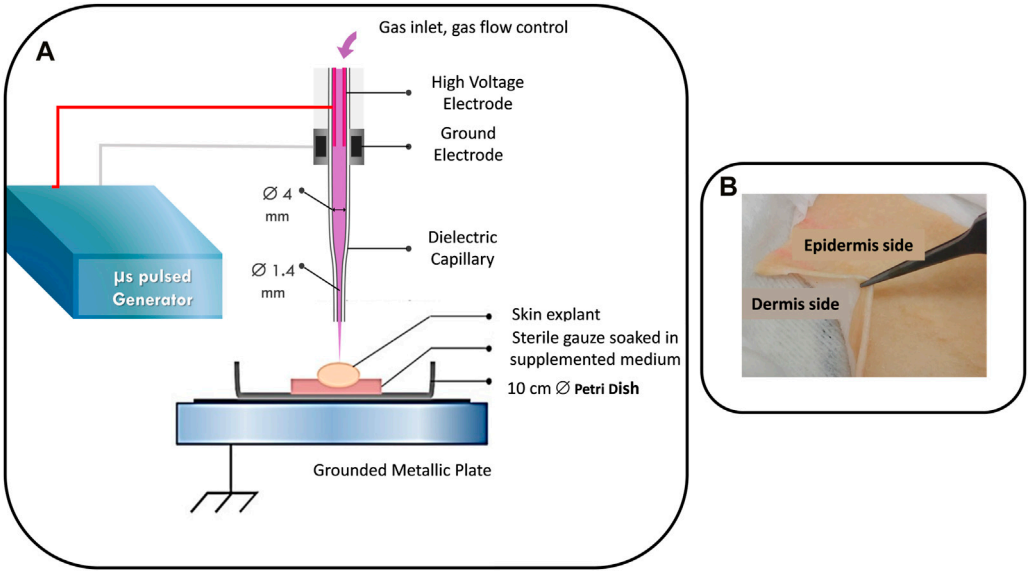

FIGURE 1
(A) Plasma gun and plasma–skin explant treatment setups. **(B)** Image of a skin explant.

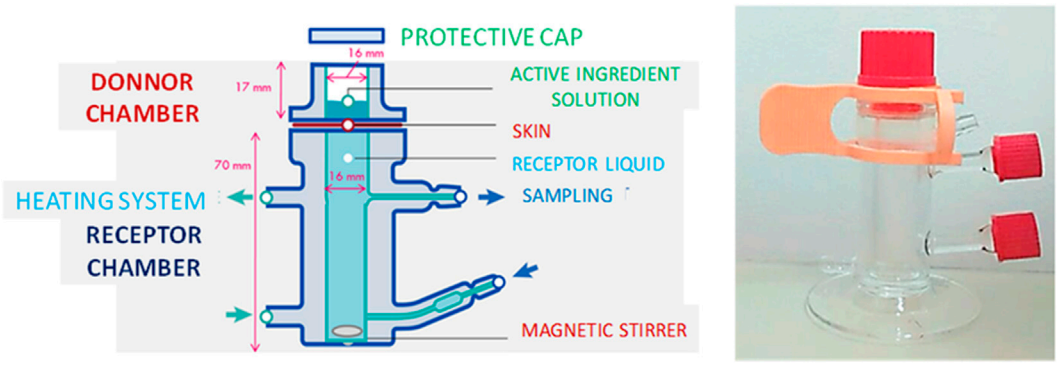

FIGURE 2
Photograph and Franz-cell setup used to measure the caffeine diffusion across the skin explant sample (schematic adapted from Biogalenys, https://www.biogalenys.com/).

including the *stratum corneum*, the epidermis, and the upper layer of the dermis. Both frozen and fresh samples were used, depending on their availability from the supplier. After receiving the skin samples in the laboratory, three 15-second consecutive baths in phosphate buffer saline (PBS, D8537, Sigma) and 70% ethanol were processed to clean them from potential pathogens and for standardization purposes. In this work, either 2 × 2 cm^2 square samples or circular punches 6–8 mm in diameter have been prepared from these cleaned large-surface samples. This allowed performing replicate experiments from the same donor.

Skin explants were then dried and set over a sterile gauze soaked with DMEM (Dulbecco's modified Eagle medium—Sigma, D5796) supplemented with 20% fetal calf serum (FCS, Sigma, F7524), 1% penicillin/streptomycin (P/S) (Sigma P0781), and 0.1% amphotericine B antifungal solution (Sigma A2942). Samples were then incubated at 37°C in a humidified atmosphere containing 5% CO_2 for at least 1 h before being used for plasma or control exposure. A daily change of the gauze and the medium mixture was performed to ensure the preservation of the explants for about 1 week. The gauze and explant were set in a 10-cm diameter Petri dish placed on a grounded metallic plate, as shown in Figure 1A.

The explants have then been plasma treated in various operating conditions. Punches have been plasma treated in their centers and then cut across the 500-µm thick direction into two half disks. The 500-µm thick surface of each of these two disks was then set over a glass slide and frozen with optimal cutting temperature compound. Transverse sections, with the top being the epidermis and the

bottom, the dermis, were then sliced with a thickness of about 7–10 μm with the help of a microtome-cryostat 350 S (Leica). The slices were then kept at −80°C before immunohistochemical analysis.

For some skin penetration experiments, following the plasma treatment, a 4.5-mm inner diameter, 6-mm high plastic cylinder was set on top of the explant kept over the gauze in the petri dish. This cylinder was tight enough to be filled with the liquid solution containing the cosmetic ingredient and kept in the CO_2 incubator from a few minutes to a few hours for studying the penetration across the sample at different times after plasma exposure.

A second set of full-thickness skin explants (Biopredic, Saint-Grégoire, France), also collected from abdominal surgery, was used for measuring hyaluronic acid penetration. These explants were washed with the same protocol as described for the dermatomized explants and incubated at 32°C in a humidified atmosphere containing 5% CO_2. Plasma treatment and/or topical application of hyaluronic acid (HA)-containing solution were processed on 8-mm diameter punches with the same cylinder described beforehand. Samples were then incubated for 1 or 6 hours at 32°C. After the plasma treatment and topical application of an HA-containing PBS solution for a different period of time, the samples were cut into two halves before being snap frozen. These samples were then analyzed by an innovative MS-MALDI technique developed in collaboration with Imabiotech (59120 Loos, France), as described in the next paragraph.

2.3 Cosmetic molecules of interest and their diffusion across a skin sample

Caffeine was used in this work, being of low molecular weight and relatively simple to dose. Moreover, caffeine is currently used in cosmetic formulations and has antioxidant properties and lipolytic properties for body-slimming purposes. Hyaluronic acid is naturally present in the skin and is involved in skin biomechanical properties, skin regulations, and treatments. It is a commonly used polymer in cosmetic products but also in esthetic treatments. Studying its penetration into the skin is of great interest. These two molecules of interest for cosmetic studies have been used. Caffeine (with a molecular weight of 194 Da) and Hyaluronic acid from Renovhyal®, Givaudan (with a molecular weight of 20 kDa) have been diluted in Dulbecco's Phosphate Buffered Saline solution (D8537, Sigma, pH 7.4) at an initial concentration of 1% (10 mg/mL). As detailed in the previous paragraph, the cosmetic ingredients were topically applied on the skin explants within the plastic cylinder both for the control group and following plasma exposure for the plasma-treated explants.

Caffeine penetration across the explant was assessed by the conventional Franz cell method. Four on-design Franz-cell assemblies (Verre Equipements, 69660 Collonges-au-Mont-d'Or) were used as shown in Figure 2. They consist of two borosilicate glass components. The upper part, called the donor chamber, contains the liquid solution with 1% caffeine. The lower portion, called the receptor chamber, consists of a double-walled borosilicate container: the inner one is filled with the PBS solution, and the outer one is flushed with a controlled-temperature water flow, ensuring a constant temperature of 32°C. The upper surface of the receptor chamber and the lower surface of the donor chamber are separated by the 2 × 2 cm^2 and 500-μm thick explant, which are held in place by a clamp. The receptor chamber is equipped with two septa. The first septum is used to collect the liquid solution (100 μL volume) at different times (ranging from a few minutes to 24 h) after topical application of the caffeine solution. The second septum is used to compensate with PBS for the collected liquid volume. The sampled solution is then analyzed with high-performance liquid chromatography (HPLC, S160 Hitachi model equipped with Chromolith (Merck 73 KGaA) 100 × 4.6 mm, 2 μm porosity column with water/methanol mobile phase.

MALDI-MSI (matrix-assisted laser desorption/ionization mass spectroscopy imaging) is a mass spectrometry imaging method leading to the space-resolved visualization of proteins, peptides, lipids, and small molecules in a cross-section of skin explants [42]. Tissue scanning by a laser beam is performed in two dimensions, while the mass spectrum is recorded. MS-MALDI-MSI was performed with the 7T MALDI-FTICR (Solarix, Bruker Daltonics, Brême, Allemagne) equipped with the SmartBeam II laser. Quantinetix 1.7.1 (ImaBiotech, France) software was used to plot the map distribution of HA. The mass-to-charge ratio (m/z) of 1180.29 corresponds to HA after a standardized enzymatic digestion [43]. Histological coloration allowed localizing the epidermis and the dermis on skin sections and by comparison, with the MALDI molecular image, to calculate the relative HA amounts according to the depth of the sample. Scanning along the cross-section of explants sample allowed determining the position of the upper surface of the *stratum corneum*, and image processing was performed to align the sample in a 2D Cartesian frame of reference. This eventually allowed for the extraction of the HA penetration profile across the 2-mm thick skin sample.

2.4 Skin analysis

Human skin surface is hydrophobic, but physical or chemical treatment may modify its wettability. A droplet digitizer (Digidrop, GBX) device was used to measure the water contact angle before and after plasma exposure of skin explants. A 5-μL deionized water droplet was automatically deposited on the skin sample at different times after plasma exposure. The accuracy and measurement reproducibility are both ± 0.1°. A minimum delay of 8 min was unfortunately imposed before the first water contact angle measurement as explants were plasma treated in a different room than that for wettability measurement.

Skin pH is also a critical parameter for revealing healthy skin. Human skin's pH is acidic, with a pH value of about 5.5. Any modification of this pH may result or reflect a modulation of cutaneous enzymatic activity, affect microbiote balance at the skin surface, epidermal desquamation, and barrier function. The pH was measured with the Skin-pH-Meter PH 905, CK Multi Probe (Courage + Khazaka electronic GmbH) with 0.1 accuracy.

The *stratum corneum*, the upper layer of skin, plays a key role in the preservation of the hydration of skin tissues. Water diffusion from the deeper layer of the epidermis, containing about 70% water, is a natural process controlled through the *stratum corneum*. This so-called transepidermal water loss (TEWL) was measured with the

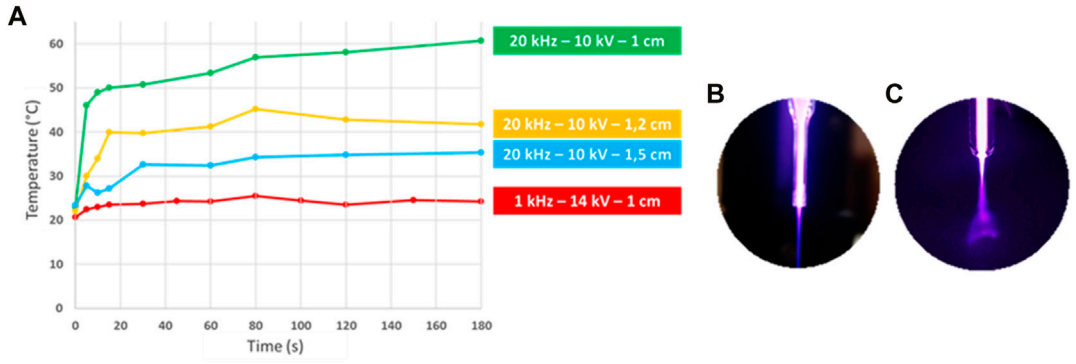

FIGURE 3
(A) Explant surface temperature evolution during 3 minutes for different plasma jet regimes. **(B)** and **(C)** are photographs of the plasma plume impinging on explant surface for 1 kHz, respectively, 20 kHz, pulse repetition rate.

Tewameter TM 300, CK Multi Probe (Courage + Khazaka electronic GmbH). Tewameter measures the water flux expressed in g/hm^2.

Beyond these surface macroscopic skin characteristics, immunofluorescence imaging was performed to assess the plasma treatment effect at the molecular level. Specific antibodies against several epidermal proteins were used to measure their expression and visualize their localization in control and plasma-exposed skin samples. Filaggrin, zonula occludens-1 (ZO-1), and involucrin expression reveal the integrity of the *stratum corneum* and epidermis. Filaggrin and involucrin are mainly abundant in the *stratum corneum,* while ZO-1, associated with the cellular junction of keratinocytes, is mainly expressed in the viable epidermis.

2.5 Statistical analysis

Each experiment was performed in triplicate with two independent repeats. All numerical data are expressed as mean ± standard deviation. Statistical analysis was performed using GraphPad Prism version 6.07 (GraphPad software) or Microsoft Excel. Differences in results were considered statistically significant when p values were lower than 0.05 (*), 0.01 (**), or 0.001 (***). Any p-value greater than 0.05 was considered statistically non-significant.

3 Results

3.1 Determination of plasma treatment protocols

The first focus of this work was to determine plasma exposure protocols to prevent any severe damage before investigating the potentialities of non-thermal plasma technology for cosmetic ingredient uptake enhancement. The first threat to the skin during plasma exposure is the thermal load.

Figure 3 presents the evolution of the temperature measured at the surface of the explants from the ignition of the plasma jet for different peak voltage amplitudes, gap distances from the capillary nozzle to the explant surface, and pulse repetition rates during a 3 min continuous exposure. The 1-kHz, 14-kV, and 1-cm setting were selected from previous *in vitro* cell permeabilization studies reported with the same plasma gun device [44]. For these operating conditions, after a rapid but very small temperature increase from room temperature (20°C) to about 23°C during the first 10 seconds of plasma exposure, a steady-state regime is reached. The balance between plasma thermal load, helium flow cooling action, and heat diffusion from the sample to the soaked gauze results in an equilibrium temperature of about 23°C. Since the heat dissipation in the investigated experimental conditions with the explant is surely different than the situation of plasma jet exposure on human skin, it can be attested that on delivery of the plasma jet on the author's hand in a static position, neither pain nor heat were felt. As the pulse repetition rate is increased to 20 kHz, the gap distance has to be controlled to avoid excessive temperature increase on skin explants. For a gap distance of 1.5 cm, the continuous and static delivery of the plasma jet results in an equilibrium temperature of about 32°C. If the gap distance is lowered to 1.2 and 1 cm, the temperature will increase to 41°C and 60°C, respectively. These latter conditions are not operable for skin exposure because they are uncomfortable and could induce tissue damage. It must be pointed out that the author's hand exposure for the 20 kHz exposure without strict control of the gap distance does not lead to such a dramatic report if the plasma nozzle is gently moved and not kept in a static position. Nevertheless, in this work where explants and not thermoregulated human skin surface were exposed, static positioning was imposed so that the 20-kHz operation was performed with a 1.5-cm gap.

As documented in Figures 3B, C, and in agreement with our previous publication [41], the increase of the pulse repetition leads to a self-induced plasma plume moving on any floating potential target. While in Figure 3B, at 1 kHz, the plasma plume over the explant is straight and very thin, with a visible impact spot diameter of about 0.5 mm; in Figure 3C, at 20 kHz, the plasma plume is much more diffuse, expanding over a 2-cm wide surface over the explant. This shift in the plasma plume topology results from the charging of the surface, its consecutive impact on the helium flow features, and the subsequent ionization wave propagation in the helium-rich

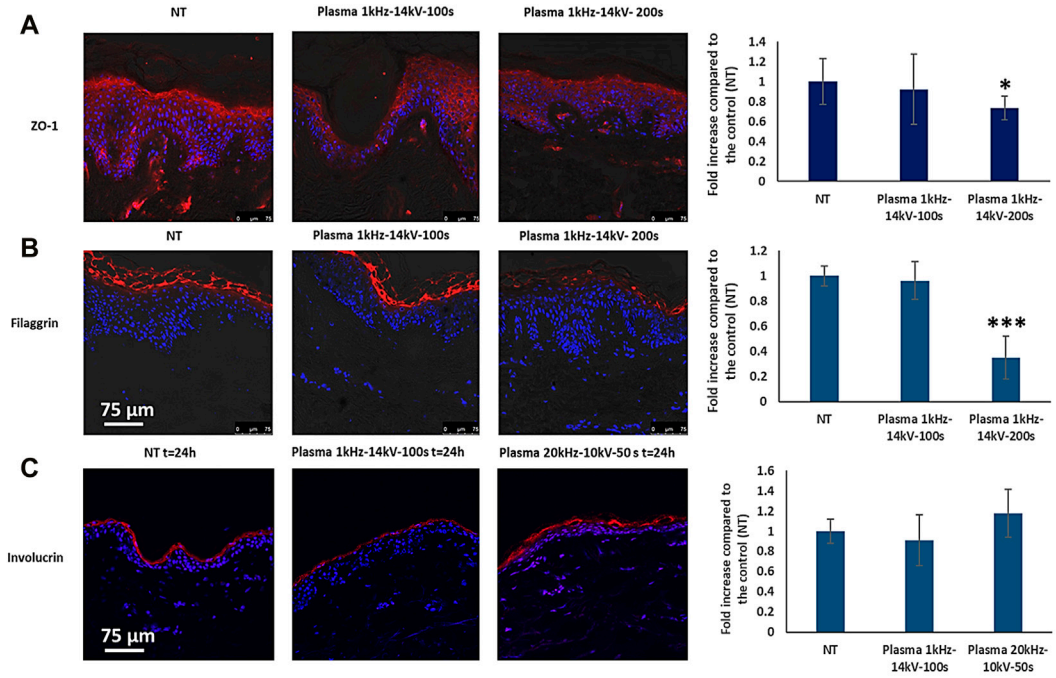

FIGURE 4
Protein fluorescence images for **(A)** ZO-1, **(B)** filaggrin, and **(C)** involucrin. The right-hand side histograms plot the fold increase of the fluorescence signal for the two plasma exposure conditions versus the control group (NT) level.

region [41]. The temperature measurements led to selecting the 1 kHz, 14 kV, 1 cm, and 20 kHz, 10 kV, 1.5 cm settings.

The next step was to assess the biological effect of such a plasma jet operation on explant tissues. Figures 4A, B, present fluorescent images and protein (ZO-1 and filaggrin) expression for control (no plasma treatment): 1 kHz, 14 kV, 1 cm, 100-s long and 1 kHz, 14 kV, 1 cm, 200-s exposures. The fluorescent microscope images show the cell nuclei in blue (DAPI labeling) and the red fluorescence of the protein markers. As explained in Section 2, the half-disk slices set on the glass slide prepared for this analysis show, on the top surface, the *stratum corneum*, which is about 10–20 µm thick, and about a 100-µm thick layer of the epidermis.

As expected, the ZO-1 fluorescence is measured in the epidermis, while the filaggrin fluorescence is confined to the *stratum corneum*. Images and their quantitative analysis reveal that the 100-s plasma exposure exhibits the same protein expression as that of the control, while a significant decrease in fluorescence is measured for the 200-s treatment. From this analysis, 200-s plasma exposure induces damage in skin explants, which may not be expected from temperature measurement alone as shown in Figure 3 where for the 1 kHz operation, the 23°C steady-state regime was measured. The involucrin expression, documented in Figure 4C, detected in the *stratum corneum* has the same level as the control and (1 kHz, 14 kV, 1 cm, 100 s) and (20 kHz, 10 kV, 1.5 cm, 50 s) exposures. This indicates that both 1 kHz and 20 kHz plasma jet operations can be safely used for skin explant exposure with controlling the gap distance and the treatment time. In the remainder of the paper, either control (only helium flow exposure) or 1k100s and 20k50s protocols will be studied.

Although not shown, a number of histological analyses of explant tissues were performed, showing no evidence for any significant destruction or lesion of the epidermis and dermis layer of the tissues for the tested plasma exposure conditions in this work.

3.2 Plasma action on skin surface characteristics

3.2.1 Transepidermal water loss

Figure 5 presents the evolution of the TEWL during 1 hour for control and 1k100s and 20k50s protocols. In the control group, only helium flow (0.5 slm and 10 mm gap to sample) was exposed for 100 s; the TEWL level was constant, ranging from 20 to 23 g/hm^2. The gas flow only delivered from the tapered capillary flushed at 0.5 slm with a gap of 1 cm from the nozzle outlet to the explant does not lead to any modulation of the *stratum corneum*, revealing that neither drying nor cooling phenomena play a significant role in the explant physiology during and following the 100-s exposure. Conversely, for the two plasma exposure protocols, a significant drop in the TEWL level is measured during and by the end of the 50/100-s plasma delivery. With the two protocols, the TEWL level then increases during the next 8 min after the end of the plasma exposure and gradually came back to the baseline level, measured at the beginning of the experiment. While in the control group, the fluctuation of the TEWL is less than 10%, the 1k100s exposure leads to a close to 20% decrease, and the 20k50s-induced decrease is about 15%. When the plasma was switched off, the 0.5 slm gas flow was also stopped, as in the control group. From Figure 3, the

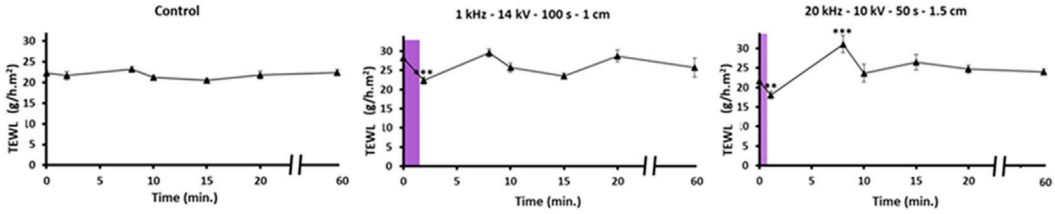

FIGURE 5
One-hour TEWL evolution for left: control, middle: 1k100s plasma exposure, and right: 20k50s plasma exposure. The violet bars visualize the plasma treatment time.

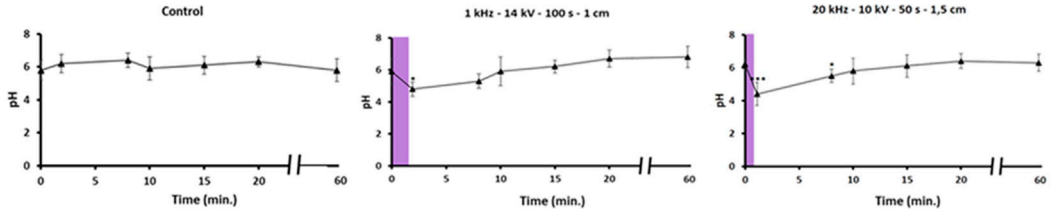

FIGURE 6
One-hour skin pH evolution for left: control, middle: 1k100s, and right: 20k50s exposures. The violet bars visualize the plasma treatment time.

temperatures at the ends of the 1k100s and 20k50s exposures are about 23°C and 32°C, respectively. Such temperatures maintained for a few tens of seconds are likely not the main reason for the TEWL decrease, this decrease being even lower for the 20k50s condition. Much more significant is the TEWL increase during the next 5–8 min following plasma exposure. Such a TEWL increase reveals that the *stratum corneum* has been disturbed by plasma exposure. This is nevertheless a transient effect, as TEWL recovers its initial level approximately ten minutes later.

3.2.2 pH

Figure 6 present the evolution of skin pH during the 1 hour following gas flow, 1k100s and 20k50s plasma exposures. The control pH fluctuates between 5.5 and 6.5, as expected for healthy human skin samples. Conversely, and as expected, the plasma exposure ends with a significant pH drop to about 4, this one being a little bit more important for the 20k50s protocol. This almost universal pH decrease when any surface is exposed to a plasma jet or a dielectric barrier discharge reveals the generation of nitrites, nitrate, and their conjugated acids. Such acidification was previously reported with the same amplitude for gelatin-mimicking tissue [44]. Following plasma switch-off and for about 20 min, the pH gradually and continuously recovers its value before explant treatment.

3.2.3 Water contact angle

Figure 7 presents the evolution of the water contact angle from 8 to 50 min after gas flow or plasma exposure. For the control samples, the wettability of the skin is almost constant, with a value for the water contact angle around 50°. Conversely, following plasma exposure, the water contact angle drops, and the skin sample turns hydrophilic with a 20° contact angle. Again, this is a transient effect, and 20 min after plasma exposure, the hydrophobicity of the skin is restored. As for pH, this is a very frequent action of non-thermal plasma exposure to induce transient hydrophilicity, usually associated with the grafting of polar radicals on the substrate [46].

In Figure 8, all three parameters (TEWL, pH, and water contact angle) have been normalized and plotted together for the two plasma protocols. The transient action of plasma exposure on the explants is thus enlightened, and the existence of a 20-minute time window is revealed, during which all the skin features experienced some modulations and were later restored to their pre-exposure levels.

3.3 Plasma-enhanced cosmetic molecule penetration

3.3.1 Caffeine uptake

Figure 9 presents the evolution of the caffeine concentration in the receptor chamber of Franz cells for explants exposed to gas flow (control) and the two 1k100s and 20k50s plasma protocols. The 1% caffeine-PBS solution is applied within the donor chamber of Franz cells right after the skin sample has been clamped in between the two Franz-cell chambers. A fourth measurement of the caffeine solution transport across the explants has been performed with first the 20k50s plasma exposure, then the clamping of the explants in the Franz cell, and waiting for 45 min before the caffeine solution filling of the donor chamber. For the control group (blue plot in Figure 9), the caffeine transport across the skin explant is delayed for about 8 h. This represents the non-plasma-assisted diffusion of caffeine solution through a 500-µm thick skin sample in our experimental conditions. It should be pointed out that active ingredient diffusion

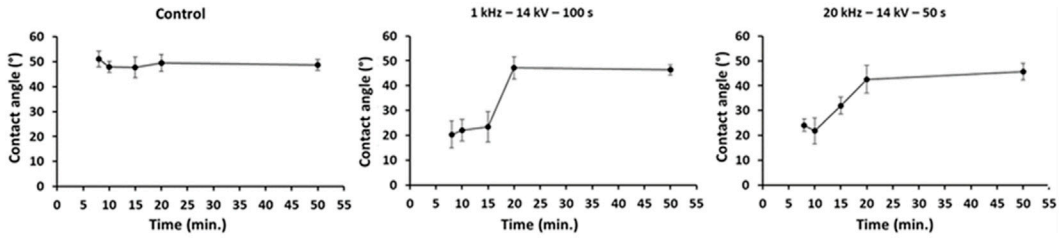

FIGURE 7
Evolution of the water contact angle for left: control, middle: 1k100s, and right: 20k50s exposures.

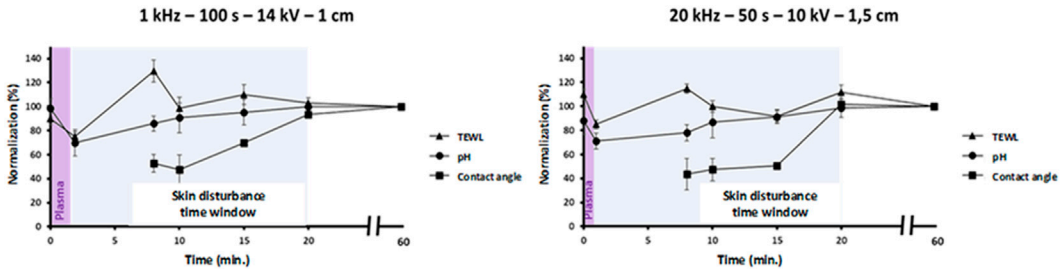

FIGURE 8
One-hour normalized evolutions of TEWL, pH, and water contact angle for left: 1k100s and right: 20k50s plasma exposures.

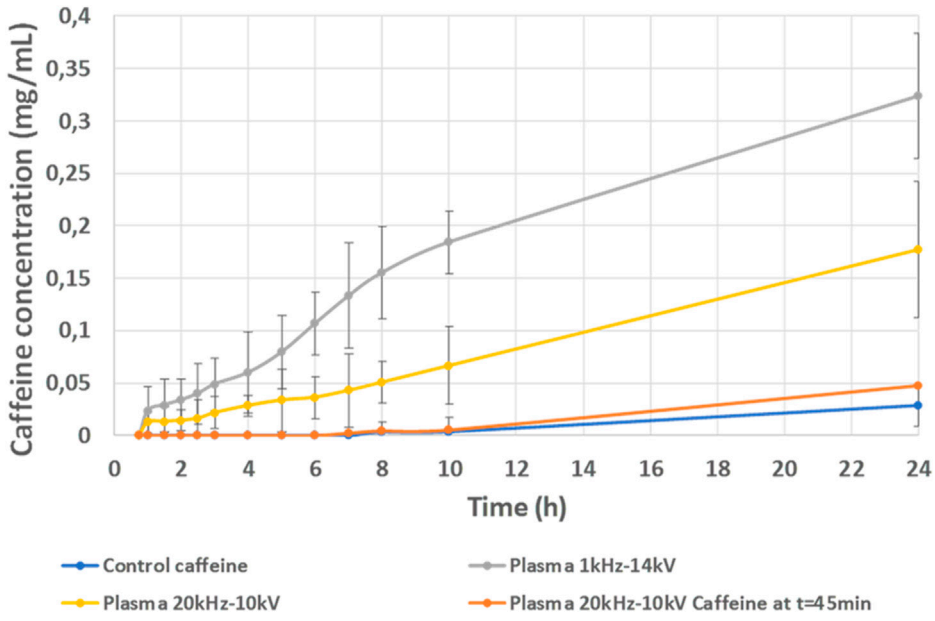

FIGURE 9
24-h evolution of the caffeine concentration measured in the receptor chamber of Franz cells for the blue plot: control, the yellow plot: 20k50s protocol with the caffeine topically applied right after the plasma exposure, the gray plot: 1k100 s protocol with the caffeine topically applied right after the plasma exposure, and the orange plot: 20k50 s protocol but caffeine topically applied with a 45-min delay after plasma exposure.

in skin samples is dependent on many parameters, such as the hair follicle density, the anatomical site, pH, concentration, and nature of the vehicle solution, and finally, on the detection limit of the diagnostic method. In Ref. [47], caffeine HPLC detection using a Franz cell setup but equipped with a dermatomized pig skin sample between donor and receptor chambers was reported to be of 0.8 µg/

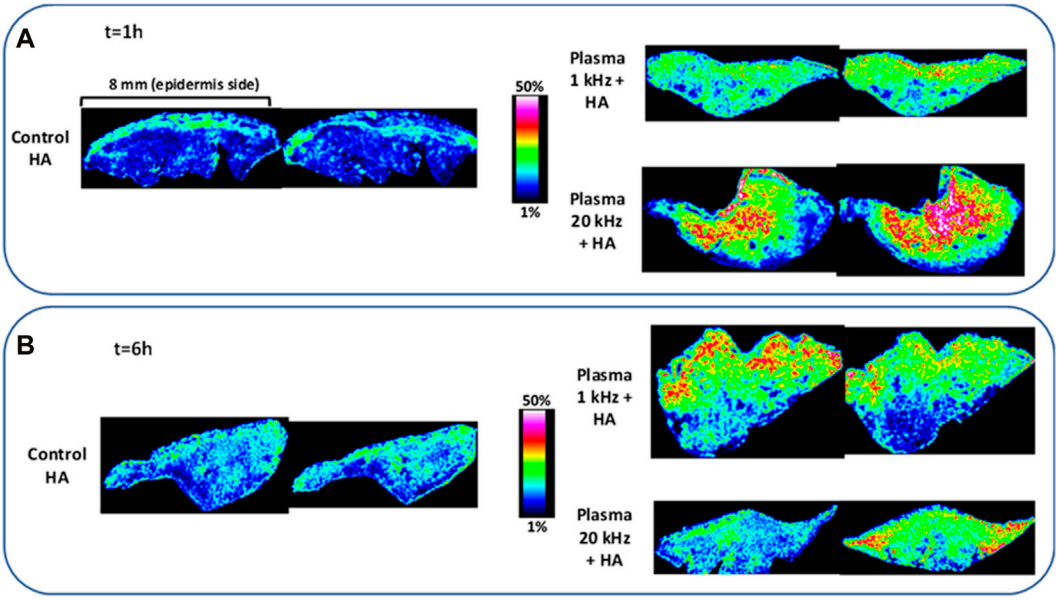

FIGURE 10
MS-MALDI skin slice images (two images for each condition) for **(A)** (top) left: control (no plasma and topical HA application for 1 h, right up: 1k100s, and right bottom: 20k50s plasma treatment and HA topical application for 1 h. **(B)** (bottom) left: control (no plasma and topical HA application for 6 h, right up: 1k100s, and right bottom: 20k50s plasma treatment and HA topical application for 6 h.

mL after 1 h and of 3.8 μg/mL after 8 h of the caffeine solution topical application. In our work, the caffeine concentration after 8 h was 3.5 μg/mL.

For plasma-treated samples, the caffeine transport is dramatically faster, being detected about 30 min after the topical application of the solution. It is worth noting that for this very early delay and whatever the plasma protocol, the caffeine concentration measured in the receptor chamber is already as high as that measured for control samples, but 24 h after topical application of the solution. This reveals the very potent plasma action on the fastening of the caffeine transport through human explants induced by a single and short duration plasma exposure. Not only is this effect measured, there is also the continuous increase in caffeine concentration in the receptor chamber during 24 h After 24 h of the plasma treatment, 15% and 30% of the pristine caffeine solution concentration is measured in the receptor chamber. It is also worth pointing out that while the two plasma protocols allow for very fast penetration of caffeine solution during the first instant, the penetration transport rate is plasma frequency dependent. The variations of the voltage, plasma power, and treatment time would also very likely induce different penetration and kinetics but were not studied in this work. The 20k100s protocol induces a linear evolution of the caffeine penetration over 24 h, while the 1k50s exposure results in a first phase ranging from about 2 to 8 h where the penetration kinetics are very high, and then a slowdown from 10 to 24 h.

The 20-minute time window corresponds to the time during which the upper surface of the skin recovers its original (prior to plasma treatment) state. The caffeine penetration measurement revealed that the transient modulation of the skin barrier (*stratum corneum*) results in an increase in the caffeine concentration in the upper layer of skin samples, but the passive diffusion in the deeper layers of the 500-μm thick explants lasts for about 30 min. This is indeed the shortest delay for which, in our experimental conditions, caffeine was detected in the Franz-cell receptor compartment. A 45-min delay was thus selected to demonstrate the transient effect of the plasma exposure so that we could be confident that the action of plasma treatment will be mostly associated with the 20-minute skin barrier modulation and that all potential deeper layer effects that could be plasma-triggered will vanish. In this latter protocol, the penetration of the caffeine follows the same profile as that for control skin samples.

3.3.2 Hyaluronic acid uptake

Figure 10 presents the MS-MALDI images of explant slices exposed to helium only and topical application of the HA solution and of those exposed to the two plasma treatment protocols before topical application of the HA solution. For every condition, two MS-MALDI images were captured. In Figure 10A, MS-MALDI images were obtained on a skin section 1 h after the HA-PBS application, while in Figure 10B, contact with the solution was maintained for 6 h before snap freezing for imaging. Following 1 h topical application, the control group exhibits an HA signal only in the upper layer of the explant. The faint HA signal imaged in the deeper layers of the epidermis and dermis probably originates from endogenous HA naturally present in human skin. Completely different MS-MALDI images are obtained for plasma-exposed explants. For 1k100s protocol, HA signal is detected all across the explants and a more intense signal is measured in the upper layer. For the 20k50s exposure, again, HA signal is measured all across the

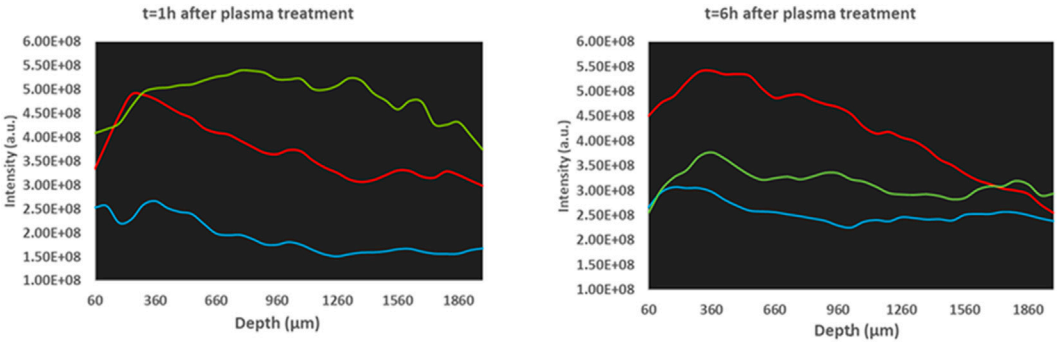

FIGURE 11
HA MS-MALDI transverse profiles for blue (control, no plasma but HA incubation), red (1k100s protocol and HA incubation), and green (20k50s and HA incubation), for left: incubation of 1 h and right: incubation of 6 h.

explants but with a higher signal intensity and with some more in-depth penetration. In Figure 10B, after 6 h of topical solution application, the HA signal in the control explants is more intense and is distributed all across the explants. This reveals the natural, non-plasma-assisted penetration of HA in human explants which require a few hours to penetrate the deeper layer of the epidermis and dermis. Following 1k100s plasma treatments and 6 h of topical solution application, the HA signal is again more intense than in Figure 10A for the same treatment, and the HA signal is again clearly more intense in the upper layer of the explants. For the 20k50s plasma treatment, the HA signal is still measured but diffuse all across the explants and weaker. For one of the explants in Figure 10B, following the 20k50s protocol with the 6-h topical solution application, it seems the HA signal starts vanishing, revealing that the HA solution has passed through the explant and that the explant is no longer permeable to the solution.

Figure 11 presents the transverse (from *stratum corneum* to dermis) profile of HA signals extracted from the images documented in Figure 10 for the three treatments (control and two plasma protocols) after 1 and 6 hours of topical solution application. The blue plot for control confirms the slow natural diffusion of the HA in human explants. The red plots for the 1k100s plasma protocol confirm that at 1 hour, the HA is mainly distributed in the upper layer, with the peak level being centered around 300 µm. For 6 h of incubation with the solution, the HA signal kept growing and diffused much deeper at a higher level than for the 1 h contact all along the 2-mm thick explant. The green plots for the 20k50s plasma protocol confirm that the penetration is faster than for the 1k100s plasma protocol. The HA signal is much higher and peaks from about 600 to 1500 µm and not around 300 µm as for the 1k100s protocol. For the 6 hours of incubation, the HA signal level has dropped and is close to that of the control group. This confirms the previously mentioned hypothesis that the HA has fully diffused across the explants and that the explants are no longer highly permeable to the HA molecule but tend to behave like the non-plasma-treated skin samples. As for the caffeine, the HA penetration rate and kinetics can not only be drastically enhanced but controlled by changing the plasma delivery protocol, as shown here with the variation of the frequency.

3.4 Air-DBD plasma for cosmetic home care

All results reported beforehand were obtained with the plasma gun device. This plasma jet was the same device used for *in vitro* cell permeabilization studies [48], for which toxicity and drug uptake kinetics were established and will be discussed in comparison with the explant treatment in the next section. The positioning of the plasma plume and the possibility to select the best protocol through the tuning of peak voltage, pulse repetition rate, gas flowrate, and gap distance were convenient and unique advantages. The two plasma protocols selected for the cosmetic ingredient uptake study correspond to low power (less than 0.9 W) helium plasma jet operations, with moderate voltage amplitude. The 20k50s regime is also almost inaudible to the human ear, and the short treatment time leads to very low helium consumption. All these characteristics are good indications for the development of a compact, safe, and low-cost-of-operation plasma jet applicator likely to be used for cosmetic application in beauty salons. Nevertheless, a preliminary test where a cheaper non-thermal plasma applicator could be used for the skin cosmetic treatment was considered in this work. This test consists of the use of the plasma ball applicator described in Section 2. Note that this later applicator costs a few euros, does not need helium feeding, being operated in ambient air, and that the very low power and short duration effectiveness that will be documented in this section are concomitant with extremely low ozone generation, whose level fall within country regulations. The objective was not to compare the efficiency of the plasma jet and the DBD applicators but to investigate the potentialities of the latter. Figure 12A presents the plasma ball treatment performed on the author's skin (on either the hand or knee) for different durations. The mean water contact angle (average of the left and right water contact angles) was assessed with a self-developed MATLAB routine applied to each photograph. For control drops set on author's skin without any plasma treatment, the water contact angle ranges from 84° to 89°. In Figure 12B, 30 s air-DBD treatment operating with a gap distance of about 1 mm was applied. A 20-µL water drop was then applied with various delays at the treatment spot, this one being about one-half square-centimeter wide. It is observed that the water contact angle substantially decreases (77%), as evidenced by the flat shape of the drop for the shorter delays after plasma treatment. The

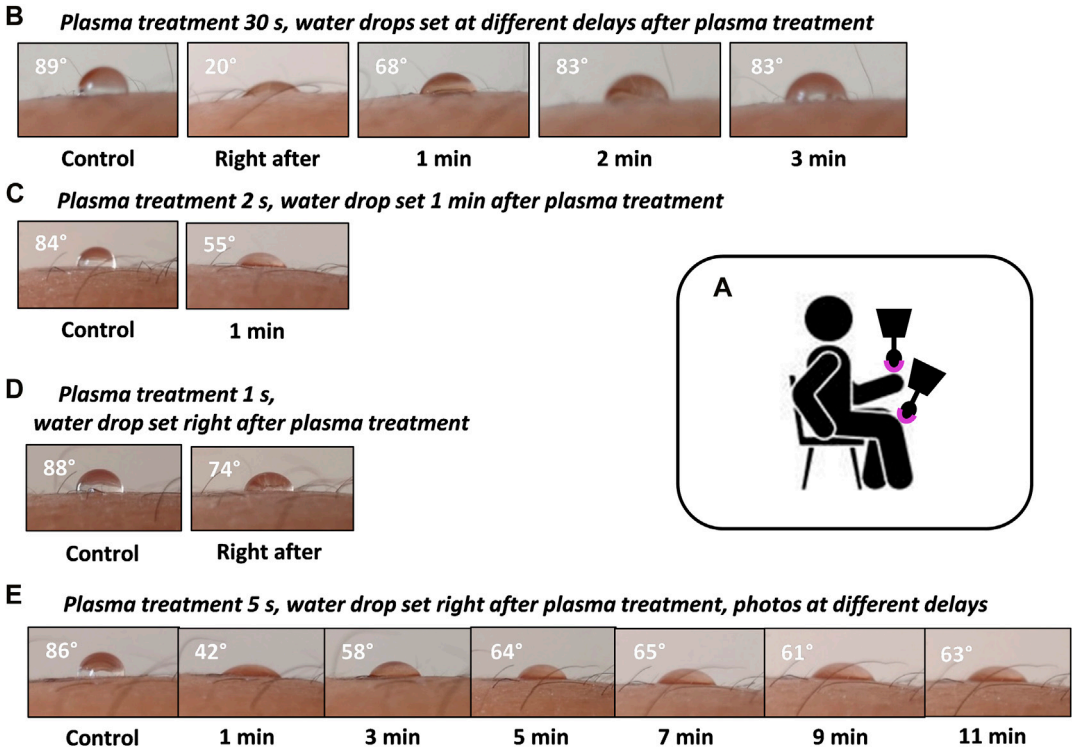

FIGURE 12
(A) Schematic for dielectric barrier discharge treatment of the hand and knee. Photographs of a 20-µL water drop set on the author's hand for **(B)** top: no plasma treatment and 30-s DBD treatment with water drop set at different delays (right after, 1, 2 and 3 min), **(C)** second row: no treatment and 2-s DBD treatment with drop set 1 min later. **(D)** Third row: no treatment and 1-s plasma treatment with drop set right after. **(E)** Bottom row: 5-s DBD treatment water drop set right after and photographs taken with a 1- to 11-min delay. The angle indicated on each photograph is the average of the left and right water contact angles.

DBD-induced skin hydrophilicity persists for about 2 min and vanishes after 3 min. For this latter delay, the drop exhibits a rounded shape as before plasma treatment (only a 7% decrease in the water contact angle in comparison with the control). Figure 12C illustrates that even a shorter, 2-s DBD application will lead to the modulation (35% decrease in water contact angle) of skin hydrophilicity, while Figure 12D indicates that a 1-second plasma delivery is still effective but much less (15% decrease). Figure 12E presents drop visualization with a different protocol, likely closer to a real cosmetic application. In Figure 12E, the DBD was delivered for 5 s, and then the water drop was applied right after plasma treatment and not at different delays as before. It is observed that the hydrophilic nature of the DBD-treated skin is preserved for more than 10 min (the water contact angle decrease evolves from 49% right after the drop is set on skin to about 27% after 11 min) with respect to the control.

Note that this is a preliminary demonstration that such a DBD plasma applicator could be later developed for cosmetic applications, based on the measurement of the transient modulation of skin hydrophilicity. This action was one of the many plasma jet actions on explants. Such modulation of skin surface was correlated with pH and TEWL transient variation when using the plasma gun. Skin hydrophilicity involves the very superficial layer of the *stratum corneum*, while TEWL modulation results from much deeper *stratum corneum* alterations. Much more work would be required to demonstrate the plasma ball's efficiency for transient transepidermal water loss modulation and subsequent cosmetic molecule uptake enhancement. Nevertheless, one may consider that plasma devices claimed to be used for cosmetic purposes (cleaning, skin moisturizing improvement, wrinkle reduction, skin disinfection, and increased absorption rate of cosmetics) are dielectric barrier discharge setups [49, 50]. Nitric oxide-safe penetration in skin explants was also reported with the DBD device [28]. The CE-certified Plasmaderm® DBD plasma device is currently routinely used in clinical studies for dermatological applications and for cancer treatment approaches [51]. The DBD-used in this work for skin wettability modulation consists of a lower power setup.

4 Conclusion and discussion

In this work, a helium plasma jet was used to expose *ex vivo* human explants for cosmetic applications.

It is reported that safe exposure can be achieved if helium flow, peak voltage amplitude, pulse repetition rate, distance to the sample, and treatment time are controlled. Simultaneously considering the temperature increase and the immunohistochemical analysis, two plasma delivery protocols are inferred: the first setting is the combination of 1 kHz frequency, 14 kV applied voltage, 100 s

treatment for a gap distance of 1 cm; the second setting is the 20 kHz, 10 kV, 50 s, and 1.5-cm gap distance. With these two protocols, the explant surface temperature was kept below 32°C for 3-min continuous plasma delivery, and no increase or decrease in representative *stratum corneum* and epidermis protein expression was measured.

The 1-kHz protocol was first chosen in correlation with our previous studies on the cell membrane permeabilization of therapeutic drugs [44]. A second pulse repetition rate of 20 kHz was also investigated, being inaudible for human ears and likely affording a larger skin surface plasma exposure [41]. The setting of the gap distance to the explant and treatment time for these two frequencies were determined from temperature measurements and adjusted to prevent any severe heating issues. The selected 1k100s and 20k50s protocols were applied for a 1-cm 14 kV and 1.5-cm 10 kV gap-peak voltage settings, respectively. They did not induce any significant modulation of protein expression in skin explants. However, these temperature and immunochemistry analyses were considered good primary indicators for safe delivery conditions with the non-thermal plasma jet. A longer plasma exposure of 200 s with the 1 kHz regime was conversely shown to induce a significant decrease of both ZO-1 and filaggrin expression (Figure 4). Therefore, this longer plasma exposure was considered too damaging for the skin and was not assessed for a cosmetic ingredient penetration study. The transient modulation of skin pH, wettability, and transepidermal water loss documented in this work with the 1k100s and 20k50s protocols were considered a secondary strong indication for a non-damaging plasma delivery on skin explants.

Individually using these two plasma delivery protocols, skin pH, skin wettability, and transepidermal water loss measurements reveal a 20-minute time window during which all these skin parameters have been modulated following plasma exposure, while helium flow has no action. This confirms that plasma delivery is safe as all investigated plasma-induced skin feature alterations vanished at the end of this time window.

In the perspective of the development of non-thermal technology for cosmetic uptake enhancement, the helium plasma jet delivery and subsequent topical application of a liquid solution containing two different molecules (caffeine and hyaluronic acid) relevant for cosmetic applications and having different molecular weights are reported. It is demonstrated that a single and short duration (50 or 100 s) plasma treatment of skin explants results in a very quick and dramatic molecule uptake increase. In comparison with the control experiments, plasma-assisted penetration reveals that each of these two molecules can be delivered across a 500-μm thick skin sample or all across a 2-mm thick explant. In our experimental conditions, caffeine penetration in plasma-treated skin after 30 min was comparable to that achieved after 8 h on untreated skin. Plasma treatment with different pulse repetition rates results in a more than ten-fold increase in the caffeine concentration measurement at 24 h after the start of the topical application. If the caffeine solution is applied with a 45-min delay after the plasma treatment, its penetration rate and kinetics are the same as for the control explants. This means that these samples, while exposed to plasma, do not show any quicker or enhanced transport of the caffeine. This is a strong indication for the transient effect of plasma treatment, not only for surface skin features but also for the transport across the explants. It seems the plasma effect has completely vanished. If any tissue microstructure would had been severely modified or if damage have been plasma-induced, the caffeine transport should have been modified, which is definitively not measured. This is again a confirmation that the skin barrier alteration triggered by the plasma delivery is transient and fully reversible, as previously reported in Ref. [35].

The same dramatic increase and pulse repetition rate-dependent uptake enhancement following plasma jet treatment is also documented for hyaluronic acid. Hyaluronic acid is detected much more quickly, 1 hour after plasma treatment, whereas 6 h are needed for non-plasma-assisted diffusion. For the 1-kHz plasma protocol, the hyaluronic concentration keeps on growing from one to 6 hours across the 2-mm thick skin samples. For the 20-kHz regime, the hyaluronic acid concentration is already at a very high level 1 hour after topical solution application, exhibiting after a 6-h incubation almost the same profile as for the control sample. This is again an indication for a non-toxic, transient plasma-induced alteration of the skin barrier.

Such transient plasma jet action was previously reported with the same helium plasma jet in the context of *in vitro* cell permeabilization and anticancer drug uptake [44]. The better uptake was achieved with a few minutes' delay between plasma delivery and drug addition in the cell culture and was demonstrated to become inoperative if a 30-min delay or longer was applied. Altogether, *ex vivo* and *in vitro* molecule uptake was shown to be triggered with enhanced kinetics following plasma jet exposure for a large variety of compounds, i.e., propidium iodide, dextran, doxorubicin, caffeine, and hyaluronic acid. It is also to be noticed that such plasma jet action was demonstrated, while the plasma jet exposed the target in a small diameter spot, over a more diffuse impact zone, or through a liquid layer for *in vitro* studies.

In this work, active ingredients were topically applied in solutions on explants and were not directly exposed to the plasma. This prevents any plasma-induced potential degradation, modification, or oxidation of the molecules of interest that may hinder efficient skin penetration. Plasma treatment of active ingredients would require some additional control experiments with plasma-treated solutions and non-plasma-treated explants. However, it is worth noting that the HPLC analysis (not shown in this work) of plasma-treated caffeine solutions revealed no degradation products, even for strong plasma exposure at 20 kHz, 14 kV, and 100 s. This may open some opportunities for plasma-assisted cosmetic active penetration in human skin, involving the plasma treatment of cosmetic formulation before their application on skin, the latter being exposed to plasma at the same time or at a different time exposed to plasma.

The transient modulation of the skin's features is finally documented *in vivo* with the use of a plasma ball dielectric barrier discharge setup on the author's skin. It is shown that skin hydrophilicity is modified following very short duration exposure from 2 to 30 s and that such alteration vanishes again a few minutes after DBD plasma delivery. In addition to this confirmed action of DBD plasma on human skin, the development of a cheap, low-cost-operation, safe, and user-friendly home care cosmetics plasma applicator is envisioned.

We can speculate that the transient modulation of skin barrier function is associated with the combined action of physical components (current, charge deposition, electric field) and reactive nitrogen and oxygen species (RNS/ROS) delivery by the plasma jet. The skin restoration may be correlated with the RNS/ROS quenching at the surface of the skin explants and the successively limited level of lipid peroxidation (measured but not documented in this work). The transient plasma action may also be associated with the very short modulation of skin features associated with the electric field and current delivered during plasma exposure. In this work, the efficient air-DBD exposure was so short (down to a few seconds). Therefore, the RNS/ROS concentration is probably extremely low, while the skin is exposed to the physical factors (electric field and current). Air-DBD-induced transient skin wettability modulation may have a different origin than the grafting of polar radicals, but it may be associated with a transient modulation of the *stratum corneum* intercellular lipid organization. The penetration of an active molecule might then be associated with the so-called intercellular pathway [37]. Such physicochemical processes were previously evoked by Wen et al. [35], but the detailed mechanics associated with skin plasma treatment will require some more work of key importance for the implementation of plasma technology in cosmetic applications.

As plasma delivery results in pH modulation, skin surface charging, and thus the generation of a charge-induced electric field, it may be considered that solution transport across the skin may have common features with those triggered by iontophoresis, as summarized in the following. During plasma delivery, different electric fields are generated and interact with the target. Typically, with the plasma jet device used in this work, transient electric fields having peak amplitudes of a few kV/cm have been measured and shown to be strongly dependent on the nature of the target [52]. The charging of the target was also documented on various targets, together with its subsequent influence on the plasma jet characteristics [53, 54]. Dezest et al. [55] studied *E. coli* bacteria inactivation when exposed to helium or helium-oxygen plasma jets. Interestingly, the comparison between helium only and helium with oxygen admixtures in plasma jet exposures led to the conclusion that reactive species were not the only species involved in *E. coli* inactivation but that an electric field and charge particles could play a significant role during helium–oxygen non-thermal plasma exposure. This interpretation was inferred from a cell membrane depolarization study revealing the likely combined effects of charged particles and an electric field. The roles of the electric field, the charge deposition, and the current during and following plasma delivery may be considered not only in contact with cells or microorganisms but also with tissues. The skin tissue includes dead and living cells, specific cell membranes, and cell junctions, so that penetration pathways [37] different from those involved in interaction with microorganisms or biofilms should be accounted for cosmetic ingredients or drug penetration.

A long-time studied physical method to promote drug or molecule uptake for dermato-cosmetic applications is iontophoresis. Iontophoresis uses a mild electric current to deliver ionized compounds present in a liquid solution into intact skin. It is an attractive modality for low-molecular weight hydrophilic solutes topical delivery. It has been demonstrated that for ionic molecules, the major action is the iontophoretic delivery, while diffusion and electro-osmosis play minor roles [9]. Nevertheless, three factors are reported to control iontophoretic flux of ionic species: an electrochemical potential gradient across the skin, the increase of skin permeability for passive transport resulting from ionotophoresis induced "skin damage," and a current-induced water flux (electro-osmosis) [56]. Interestingly, the latter two factors can also affect the transport of neutral solutions, as proven with the glucose transport study. In Ref. [57], it is also mentioned that the ion transport is enhanced during iontophoresis, but secondary effects such as convective solvent flow and biological membrane permeability increase due to the applied electric field, which may also contribute to the flux increase. Uncharged molecules transport can also be affected, enhanced, or delayed depending on the polarity of the applied field. A detailed study of mannitol transport across the human epidermal membrane reveals that the solution flow velocity is proportional to the magnitude of the applied field. Membrane alterations were reported for the highest applied voltage (1 V in this study), and these changes appeared to reverse over time. The impact of the pH value is also documented and critical for such transport with microcurrent applicators developed for iontophoresis. In Ref. [58], it is reported that at pH 7.4, the human or pig skin is negatively charged and selectively permeable to cations. Such negative charging can be reduced, neutralized, or even reversed when iontophoresis is applied. pH modulation impact is also reported, as an example, as follows: at physiological pH, the mannitol transport is cation-selective dominant at the first time when the skin is negatively charged, while by lowering the pH to 3.5, the electro-osmosis reverses, the skin surface turning positively charged and thus the transport becoming anion selective.

The biological impact of the electric field delivered by non-thermal plasma (plasma jet or DBD) resulting from charge deposition on target has so far not been investigated in detail and is evidently strongly dependent on the nature of the sample. The confirmation of the analogy between plasma delivery and ionotophoresis during skin treatment proposed in this work will require such future characterization.

Data availability statement

The original contributions presented in the study are included in the article/Supplementary Material, further inquiries can be directed to the corresponding author.

Author contributions

VV, CH, CP, J-MP, and ER were involved in the experimental design, data collection and analysis, and writing of the manuscript. SD was involved in the experimental design, data collection, and editing of the manuscript. OJ was involved in the MALDI-MS imaging experiments and manuscript writing. CN was involved in the experimental design, data analysis, and editing of the manuscript AS was involved in data collection, analysis, and editing of the manuscript. All authors contributed to the article and approved the submitted version.

Funding

This work and VV were supported by LVMH CIFRE ANRT n° 2017/0743. This work was supported by CNRS GDR 2025 HAPPYBIO.

Acknowledgments

The authors thank Imabiotech, in particular, Raphaël Legouffe and David Bonnel, for their very valuable technical contribution to HA MS-MALDI imaging. The authors also express their sincere appreciation to Sylvianne Schnebert for supporting the development of this work and for her critical analysis of the results.

Conflict of interest

The authors declare that the research was conducted in the absence of any commercial or financial relationships that could be construed as a potential conflict of interest.

Publisher's note

All claims expressed in this article are solely those of the authors and do not necessarily represent those of their affiliated organizations, or those of the publisher, the editors, and the reviewers. Any product that may be evaluated in this article, or claim that may be made by its manufacturer, is not guaranteed or endorsed by the publisher.

References

1. Shahbandeh M, Value of the cosmetics market worldwide from 2018 to 2025 (in billion U.S. Dollars). (2019). Available from: https://www.statista.com/statistics/585522/global-value-cosmetics-market/.

2. Mahdavi H, Kermani Z, Faghihi G, Asilian A, Hamishehkar H, Jamshidi A. Preparation and evaluation of cosmetic patches containing lactic and glycolic acids. *Indian J Dermatol Venereol Leprol* (2006) 72:432–6. doi:10.4103/0378-6323.29339

3. El-Domyati M, S El-Ammawi T, Moawad O, El-Fakahany H, Medhat W, Mahoney MG, et al. Efficacy of mesotherapy in facial rejuvenation: A histological and immunohistochemical evaluation. *Int J Dermatol* (2012) 51(8):913–9. doi:10.1111/j.1365-4632.2011.05184.x

4. Bal SM, Caussin J, Pavel S, Bouwstra JA. *In vivo* assessment of safety of microneedle arrays in human skin. *Eur J Pharm Sci* (2008) 35(3):193–202. doi:10.1016/j.ejps.2008.06.016

5. Badran MM, Kuntsche J, Fahr A. Skin penetration enhancement by a microneedle device (Dermaroller®) *in vitro*: Dependency on needle size and applied formulation. *Eur J Pharm Sci* (2009) 36(4–5):511–23. doi:10.1016/j.ejps.2008.12.008

6. Escobar-Chávez JJ, Bonilla-Martínez D, Villegas-González MA, Rodríguez-Cruz IM, Domínguez-Delgado CL. The use of sonophoresis in the administration of drugs throughout the skin. *J Pharm Pharm Sci* (2009) 12(1):88–115. doi:10.18433/j3c30d

7. Alvarez-Román R, Merino G, Kalia YN, Naik A, Guy RH. Skin permeability enhancement by low frequency sonophoresis: Lipid extraction and transport pathways. *J Pharm Sci* (2003) 92(6):1138–46. doi:10.1002/jps.10370

8. Park D, Park H, Seo J, Lee S. Sonophoresis in transdermal drug deliverys. *Ultrasonics* (2014) 54(1):56–65. doi:10.1016/j.ultras.2013.07.007

9. Patravale VB, Mandawgade SD. Novel cosmetic delivery systems: An application update. *Int J Cosmet Sci* (2008) 30(1):19–33. doi:10.1111/j.1468-2494.2008.00416.x

10. Zhang L, Lerner S, Rustrum WV, Hofmann GA. Electroporation-mediated topical delivery of vitamin C for cosmetic applications. *Bioelectrochemistry Bioenerg* (1999) 48(2):453–61. doi:10.1016/s0302-4598(99)00026-4

11. Murthy SN, Sammeta SM, Bowers C. Magnetophoresis for enhancing transdermal drug delivery: Mechanistic studies and patch design. *J Control Release* (2010) 148(2):197–203. doi:10.1016/j.jconrel.2010.08.015

12. Alegre-Sánchez A, Jiménez-Gómez N, Boixeda P. Laser-assisted drug delivery. *Actas Dermosifiliogr (Engl Ed* (2018) 109:858. doi:10.1016/j.ad.2018.07.008

13. Khlyustova A, Labay C, Machala Z, Ginebra M-P, Canal C. Important parameters in plasma jets for the production of RONS in liquids for plasma medicine: A brief review. *Front Chem Sci Eng* (2019) 13(2):238–52. doi:10.1007/s11705-019-1801-8

14. Graves DB. Reactive species from cold atmospheric plasma: Implications for cancer therapy. *Plasma Process Polym* (2014) 11(12):1120–7. doi:10.1002/ppap.201400068

15. Weidinger A, Kozlov AV. Biological activities of reactive oxygen and nitrogen species: Oxidative stress versus signal transduction. *Biomolecules* (2015) 5(2):472–84. doi:10.3390/biom5020472

16. Robert E, Darny T, Dozias S, Iseni S, Pouvesle J-M. New insights on the propagation of pulsed atmospheric plasma streams: From single jet to multi jet arrays. *Phys Plasmas* (2015) 22:122007. doi:10.1063/1.4934655

17. Obradovic BM, Ivković SS, Kuraica MM. Spectroscopic measurement of electric field in dielectric barrier discharge in helium. *Appl Phys Lett* (2008) 92(19):191501. doi:10.1063/1.2927477

18. Bourdon A, Darny T, Pechereau F, Pouvesle J-M, Viegas P, Iséni S, et al. Numerical and experimental study of the dynamics of a μs helium plasma gun discharge with various amounts of N2 admixture. *Plasma Sourc Sci. Technol.* (2016) 25:035002. doi:10.1088/0963-0252/25/3/035002

19. Kubinova S, Zaviskova K, Uherkova L, Zablotskii V, Churpita O, Lunov O, et al. Non-thermal air plasma promotes the healing of acute skin wounds in rats. *Sci Rep* (2017) 7:45183. doi:10.1038/srep45183

20. Haertel B, von Woedtke T, Weltmann KD, Lindequist U. Non-thermal atmospheric-pressure plasma possible application in wound healing. *Biomol Ther (Seoul)* (2014) 22(6):477–90. doi:10.4062/biomolther.2014.105

21. Heinlin J, Zimmermann JL, Zeman F, Bunk W, Isbary G, Landthaler M, et al. Randomized placebo-controlled human pilot study of cold atmospheric argon plasma on skin graft donor sites. *Wound Repair Regen* (2013) 21(6):800–7. doi:10.1111/wrr.12078

22. Daeschlein G, Scholz S, Ahmed R, Majumdar A, von Woedtke T, Haase H, et al. Cold plasma is well-tolerated and does not disturb skin barrier or reduce skin moisture. *J Dtsch Dermatol Ges* (2012) 10(7):509–15. doi:10.1111/j.1610-0387.2012.07857.x

23. Heinlin J, Isbary G, Stolz W, Morfill G, Landthaler M, Shimizu T, et al. Plasma applications in medicine with a special focus on dermatology. *J Eur Acad Dermatol Venereol* (2011) 25(1):1–11. doi:10.1111/j.1468-3083.2010.03702.x

24. Zhai S-y, Kong MG, Xia Y. Cold atmospheric plasma ameliorates skin diseases involving reactive oxygen/nitrogen species-mediated functions. *Front Immunol* (2022) 13:868386. doi:10.3389/fimmu.2022.868386

25. Szili EJ, Harding FJ, Hong S-H, Herrmann F, Voelcker NH, Short RD. The hormesis effect of plasma-elevated intracellular ROS on HaCaT cells. *J Phys Appl Phys* (2015) 48. doi:10.1088/0022-3727/48/49/495401

26. Balzer J, Heuer K, Demir E, Hoffmanns MA, Baldus S, Fuchs PC, et al. Non-thermal dielectric barrier discharge (DBD) effects on proliferation and differentiation of human fibroblasts are primary mediated by hydrogen peroxide. *PLoS One* (2015) 10(12):e0144968. doi:10.1371/journal.pone.0144968

27. Borchardt T, Ernst J, Helmke A, Tanyeli M, Schilling AF, Felmerer G, et al. Effect of direct cold atmospheric plasma (diCAP) on microcirculation of intact skin in a controlled mechanical environment. *Microcirculation* (2017) 24(8):e12399. doi:10.1111/micc.12399

28. Fuchs C, Awakowicz P, Suschek CV, Oplander C, Volkmar CM, Rohle M, et al. The topical use of nonthermal dielectric barrier discharge (DBD): Nitric oxide related effects on human skin. *Nitric Oxide* (2015) 44:52–60. doi:10.1016/j.niox.2014.11.015

29. Maho T, Binois R, Brulé-Morabito F, Demasure M, Douat C, Dozias S, et al. Anti-bacterial action of plasma multi-jets in the context of chronic wound healing. *Appl Sci* (2021) 11(20):9598. doi:10.3390/app11209598

30. Morabit Y, Hasan MI, Whalley RD, Robert E, Modic M, Walsh JL. A review of the gas and liquid phase interactions in low-temperature plasma jets used for biomedical applications. *The Eur Phys J D* (2021) 75(1):32–26. doi:10.1140/epjd/s10053-020-00004-4

31. Daeschlein G, Scholz S, Ahmed R, von Woedtke T, Haase H, Niggemeier M, et al. Skin decontamination by low-temperature atmospheric pressure plasma jet and dielectric barrier discharge plasma. *J Hosp Infect* (2012) 81(3):177–83. doi:10.1016/j.jhin.2012.02.012

32. Ali A, Kim YH, Lee JY, Lee S, Uhm HS, Cho G, et al. Inactivation of Propionibacterium acnes and its biofilm by non-thermal plasma. *Curr Appl Phys* (2014) 14:S142–8. doi:10.1016/j.cap.2013.12.034

33. Fluhr JW, Sassning S, Lademann O, Darvin ME, Schanzer S, Kramer A, et al. *In vivo* skin treatment with tissue-tolerable plasma influences skin physiology and antioxidant profile in human *stratum corneum*. *Exp Dermatol* (2012) 21(2):130–4. doi:10.1111/j.1600-0625.2011.01411.x

34. Athanasopoulos DK, Svarnas P, Gerakis A. Cold plasma bullet influence on the water contact angle of human skin surface. *J Electrost* (2019) 102:103378. doi:10.1016/j.elstat.2019.103378

35. Wen X, Xin Y, Hamblin MR, Jiang X. Applications of cold atmospheric plasma for transdermal drug delivery: A review. *Drug Deliv Transl Res* (2021) 11(3):741–7. doi:10.1007/s13346-020-00808-2

36. Xin Y, Wen X, Hamblin MR, Jiang X. Transdermal delivery of topical lidocaine in a mouse model is enhanced by treatment with cold atmospheric plasma. *J Cosmet Dermatol* (2021) 20:626–35. doi:10.1111/jocd.13581

37. Busco G, Robert E, Chettouh-Hammas N, Pouvesle J-M, Grillon C. The emerging potential of cold atmospheric plasma in skin biology. *Free Radic Biol Med* (2020) 161:290–304. doi:10.1016/j.freeradbiomed.2020.10.004

38. von Woedtke T. *Oral invited Communication, Translation from plasma medicine achievements to cosmetics*. Orléans, France: IMPCS International Meeting for Plasma Cosmetic Science (2019).

39. Lu X, Bruggeman PJ, Reuter S, Naidis G, Bogaerts A, Laroussi M, et al. Grand challenges in low temperature plasmas. *Front Phys* (2022) 1036. doi:10.3389/fphy.2022.1040658

40. Robert E, Barbosa E, Dozias S, Vandamme M, Cachoncinlle C, Viladrosa R, et al. Experimental study of a compact nanosecond plasma gun. *Plasma Process Polym* (2009) 6(12):795–802. doi:10.1002/ppap.200900078

41. Omran AV, Busco G, Ridou L, Dozias S, Grillon C, Pouvesle J-M, et al. Cold atmospheric single plasma jet for RONS delivery on large biological surfaces. *Plasma Sourc Sci Tech* (2020) 29(10):105002. doi:10.1088/1361-6595/abaffd

42. Bonnel D, Legouffe R, Eriksson AH, Mortensen RW, Pamelard F, Stauber J, et al. MALDI imaging facilitates new topical drug development process by determining quantitative skin distribution profiles. *Anal Bioanal Chem* (2018) 410(11):2815–28. doi:10.1007/s00216-018-0964-3

43. Legouffe R, Jeanneton O, Gaudin M, Tomezyk A, Gerstenberg A, Dumas M, et al. Hyaluronic acid detection and relative quantification by mass spectrometry imaging in human skin tissues. *Anal Bioanal Chem* (2022) 414(19):5781–91. doi:10.1007/s00216-022-04139-8

44. Vijayarangan V, Delalande A, Dozias S, Pouvesle J-M, Pichon C, Robert E. Cold atmospheric plasma parameters investigation for efficient drug delivery in HeLa cells. *IEEE Trans Radiat Plasma Med Sci* (2017) 2(2):109–15. doi:10.1109/TRPMS.2017.2759322

45. Busco G, Omran AV, Ridou L, Pouvesle J-M, Robert E, Grillon C. Cold atmospheric plasma-induced acidification of tissue surface: Visualization and quantification using agarose gel models. *J Phys D: Appl Phys* (2019) 52(24):24LT01. doi:10.1088/1361-6463/ab1119

46. Wang R, Shen Y, Zhang C, Yan P, Shao T. Comparison between helium and argon plasma jets on improving the hydrophilic property of PMMA surface. *Appl Surf Sci* (2016) 367:401–6. doi:10.1016/J.APSUSC.2016.01.199

47. Salmon D, Gilbert E, Gioia B, Haftek M, Pivot C, Verrier B, et al. New easy handling and sampling device for bioavailability screening of topical formulations. *Eur J Dermatol* (2015) 25(1):23–9. doi:10.1684/ejd.2015.2551

48. Vijayarangan V, Delalande A, Dozias S, Pouvesle J-M, Robert E, Pichon C. New insights on molecular internalization and drug delivery following plasma jet exposures. *Int J Pharmaceutics* (2020) 589:119874. doi:10.1016/j.ijpharm.2020.119874

49. youtube.com (2022). Available at: https://www.youtube.com/watch?v=O8m4kS6OFj0 (Accessed October 5, 2022).

50. Gelker M, Mrotzek J, Ichter A, Müller-Goymann CC, Viöl W. Influence of pulse characteristics and power density on *stratum corneum* uptake by dielectric barrier discharge. *Biochim Biophys Acta (Bba) - Gen Subjects* (2019) 1863(10):1513–23. doi:10.1016/j.bbagen.2019.05.014

51. Bernhardt T, Semmler ML, Schäfer M, Bekeschus S, Emmert S, Boeckmann L. Plasma medicine: Applications of cold atmospheric pressure plasma in dermatology. *Oxidative Med Cell Longevity* (2019) 2019:3873928. doi:10.1155/2019/3873928

52. Darny T, Pouvesle J-M, Puech V, Douat C, Dozias S, Robert E. Analysis of conductive target influence in plasma jet experiments through helium metastable and electric field measurements. *Plasma Sourc Sci Tech* (2017) 26(4):045008. doi:10.1088/1361-6595/aa5b15

53. Darny T, Pouvesle J-M, Fontane J, Joly L, Dozias S, Robert E. Plasma action on helium flow in cold atmospheric pressure plasma jet experiments. *Plasma Sourc Sci. Technol.* (2017) 26:105001. doi:10.1088/1361-6595/aa8877

54. Guaitella O, Sobota A. The impingement of a kHz helium atmospheric pressure plasma jet on a dielectric surface. *J Phys D: Appl Phys* (2015) 48:255202. doi:10.1088/0022-3727/48/25/255202

55. Dezest M, Bulteau A-L, Quinton D, Chavatte L, Le Bechec M, Cambus J-P, et al. Oxidative modification and electrochemical inactivation of *Escherichia coli* upon cold atmospheric pressure plasma exposure. *PLoS ONE* (2017) 12(3):e0173618. doi:10.1371/journal.pone.0173618

56. Marro D, Kalia YN, Delgado-Charro MB, Guy RH. Contributions of electromigration and electro-osmosis to iontophoretic drug delivery. *Pharm Res* (2001) 18:1701–8. doi:10.1023/A:1013318412527

57. Sims SM, Higuchi WI, Srinivasan V. Skin alteration and convective solvent flow effects during iontophoresis: I. Neutral solute transport across human skin. *Int J Pharmaceutics* (1991) 69(2):109–21. doi:10.1016/0378-5173(91)90216-B

58. Marro D, Guy RH, Begoña Delgado-Charro M. Characterization of the iontophoretic permselectivity properties of human and pig skin. *J Controlled Release* (2001) 70(1-2):213–7. doi:10.1016/s0168-3659(00)00350-3